Regularization of Numerical Interface Thickness in UCLS Simulations of Transport Processes in Bubbles *

Néstor Balcázar-Arciniega[1][0000−0003−0776−2086], Joaquim Rigola[1][0000−0002−6685−3677], and Assensi Oliva[1][0000−0002−2805−4794]

[1] Heat and Mass Transfer Technological Center (CTTC), Universitat Politècnica de Catalunya-BarcelonaTech (UPC). Colom 11, 08222, Terrassa (Barcelona), Spain
nestor.balcazar@upc.edu, nestorbalcazar@yahoo.es

Abstract. This work investigates how numerical interface thickness affects Direct Numerical Simulations (DNS) of bubble hydrodynamics and interfacial mass transfer within an Unstructured Conservative Level-Set (UCLS) framework. In UCLS, fluid properties and surface-tension forces are regularized across a diffuse interface of thickness controlled by $\varepsilon = 0.5\,h^{\alpha}$, where h is a local mesh-length measure and α is a tunable exponent. A sensitivity analysis is performed for a gravity-driven rising bubble to quantify the influence of α on the terminal Reynolds number and Sherwood number. The results show that moderate variations in interface thickness have a limited impact on these integral quantities, while excessively aggressive settings may reduce numerical robustness. The study provides practical guidance for selecting α in UCLS simulations of coupled hydrodynamics and transport processes in bubbles.

Keywords: Bubbles · Mass transfer · Unstructured Conservative Level-Set Method · Finite-Volume Method · Unstructured Meshes · Unstructured Flux-Limiters · Direct Numerical Simulation · High-Performance Computing

1 Introduction

Bubbly flows and interfacial transport processes are ubiquitous in nature and industry, governing the performance of a wide range of systems from thermal power-plant equipment (e.g., steam generators and cooling towers) to chemical-engineering unit operations and multiphase reactors.

Experimental research of bubbly flows is constrained by the optical access, while analytical approaches rely on simplifying the physics. With the growth of high performance computing, Direct Numerical Simulation (DNS) [7,9,8] of bubbly flows has been empowered. However, DNS of two-phase flows remains challenging: it requires controlling numerical diffusion and spurious oscillations near discontinuities, accurately

* The principal author, N. Balcázar-Arciniega, acknowledges financial support from the Government of Catalonia through the Serra Húnter Programme (UPC-LE8027). Simulations were performed on the MareNostrum 5 supercomputer at the BSC (Barcelona, Spain), using computing resources allocated by the RES projects IM-2025-2-0019. The authors acknowledge the financial support of the MCIN/AEI under the project PID2023-153281OB-I00, Spain.

ICCS Camera Ready Version 2026
To cite this paper please use the final published version:
DOI: 10.1007/978-3-032-29918-5_16

evaluating surface-tension forces, and ensuring robustness under large density and viscosity contrasts, all while maintaining feasible computational cost.

In the Unstructured Conservative Level-Set (UCLS) method [4,5,3,6,7,9,8], physical properties are regularized through smoothed Heaviside functions and surface-tension forces are concentrated near the interface using a smoothed Dirac delta, both constructed from the marker function. This construction defines a numerical interface thickness controlled by the parameter $\varepsilon = 0.5\,h^{\alpha}$, where h denotes a local mesh-length measure and α is a tunable exponent. While a sufficiently thick interface may improve robustness (e.g., curvature evaluation and stability), excessive regularization can smear interfacial gradients and bias integral quantities such as drag-related measures and transfer rates. Conversely, overly thin interfaces may increase sensitivity to mesh irregularity and amplify numerical noise on unstructured grids. Despite the practical importance of this accuracy-robustness trade-off, a systematic assessment of how ε impacts the bubble hydrodynamics and interfacial mass transfer within UCLS is still limited.

The objective of this work is to quantify the sensitivity of the terminal Reynolds number and the Sherwood number, to the numerical interface thickness in UCLS-based DNS of hydrodynamics and mass transfer in rising bubbles.

2 Mathematical Formulation and Numerical Methods

2.1 Incompressible two-phase flow and UCLS method

The incompressible two-phase flow follows the one-fluid formulation

$$\frac{\partial}{\partial t}(\rho\mathbf{v}) + \nabla\cdot(\rho\mathbf{v}\mathbf{v}) = -\nabla p + \nabla\cdot\left[\mu\left(\nabla\mathbf{v} + (\nabla\mathbf{v})^{T}\right)\right] + (\rho-\rho_0)\mathbf{g} + \mathbf{f}_{\sigma},\ \nabla\cdot\mathbf{v} = 0, \quad (1)$$

where p is pressure, $\mathbf{v}$ velocity, ρ density, μ viscosity, $\mathbf{g}$ gravity, and $\mathbf{f}_{\sigma}$ the surface-tension force per unit volume, ρ and μ are constant for each phase. In Ω, $\rho = \rho_c H_c + \rho_d H_d$, $\mu = \mu_c H_c + \mu_d H_d$. H_c the Heaviside function equal to one in Ω_c and zero elsewhere, $H_d = 1 - H_c$. If periodic boundary conditions are applied along the y-axis (aligned with $\mathbf{g}$), then $\rho_0 = \frac{1}{V_{\Omega}}\int_{\Omega}(\rho_c H_c + \rho_d H_d)\,dV$ [7,3,9]; otherwise $\rho_0 = 0$.

Interface capturing is performed with the finite-volume UCLS method [7,4,5,9,8] on 3D collocated unstructured meshes. The multi-marker UCLS formulation prevents the numerical coalescence [7,3,9]. Each bubble is represented by the UCLS marker $\phi_i = \frac{1}{2}\left(\tanh\left(\frac{d_{\Gamma,i}}{2\varepsilon}\right) + 1\right)$, $i = 1, 2, \ldots, N_m$, where $d_{\Gamma,i}$ is a signed distance function and ε an interface thickness parameter. The advection and re-initialization equations are:

$$\frac{\partial\phi_i}{\partial t} + \nabla\cdot(\phi_i\mathbf{v}) = 0,\ \frac{\partial\phi_i}{\partial\tau} + \nabla\cdot\left(\phi_i(1-\phi_i)\,\mathbf{n}_i^{*}\right) = \nabla\cdot(\varepsilon\nabla\phi_i)\,, \quad (2)$$

where the unstructured re-initialization equation [4,5,7,9,8] is solved in pseudo-time τ until steady state, $\mathbf{n}_i^{*}$ denotes the interface normal at $\tau = 0$. Inverting ϕ_i yields $d_{\Gamma,i}(\phi_i) = \varepsilon\ln\left(\frac{\phi_i}{1-\phi_i}\right)$, so that the distance between $\phi_{i,1}$ and $\phi_{i,2}$ is $w_{\Gamma,i} = d_{\Gamma,i}(\phi_{i,2}) - d_{\Gamma,i}(\phi_{i,1}) = \varepsilon\left[\ln\left(\frac{\phi_{i,2}}{1-\phi_{i,2}}\right) - \ln\left(\frac{\phi_{i,1}}{1-\phi_{i,1}}\right)\right]$. For $\phi_{i,1} = 0.05$ and $\phi_{i,2} = 0.95$, the thickness gives $w_{\Gamma,i} = 2\varepsilon\ln(19) \approx 5.889\,\varepsilon$. At Ω_P, $\varepsilon_P = 0.5\,h_P^{\alpha}$ [4,5,7,9,8], where

ICCS Camera Ready Version 2026
To cite this paper please use the final published version:
DOI: 10.1007/978-3-032-29918-5_16

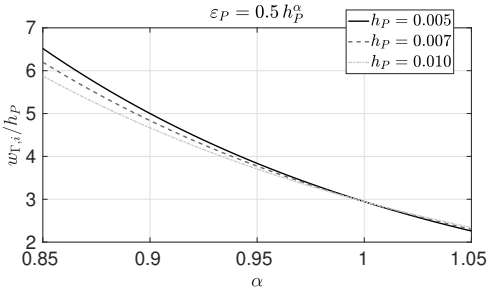

Fig. 1. Normalized numerical interface thickness $w_{\Gamma,i}/h_P$ for $\varepsilon_P = 0.5\,h_P^\alpha$, for characteristic grid-size h_P (see legend). $\alpha = 1$ yields a grid-independent thickness measured in number of cell sizes, whereas $\alpha \neq 1$ introduces a mesh dependence.

h_P is the local grid-size and α is a tunable parameter. The normalized interface thickness is $\frac{w_{\Gamma,i}}{h_P} = \ln(19)\,h_P^{\alpha-1}$. Figure 1 depicts that $\alpha = 1$ keeps $w_{\Gamma,i}/h_P$ constant under grid refinement, whereas $\alpha \neq 1$ introduces a mesh dependence $w_{\Gamma,i}/h_P \propto h_P^{\alpha-1}$ (e.g., $w_{\Gamma,i}/h_P \propto h_P^{-0.1}$ for $\alpha = 0.9$). The re-initialization equation is advanced with $\Delta\tau = C_\tau \min_P\left(\frac{h_P^2}{\varepsilon_P}\right)$, with $C_\tau = 0.05$ [4,5,7,9,8], and a single re-initialization step.

2.2 Surface-tension force and species transport

Interface normals and curvatures are calculated as $\mathbf{n}_i = \frac{\nabla\phi_i}{\|\nabla\phi_i\|}$, $\kappa_i = -\nabla\cdot\mathbf{n}_i$. The Continuous Surface Force (CSF) approach [10] calculates the surface tension, in the UCLS framework [3,6,7,9,8]: $\mathbf{f}_\sigma = \sum_{i=1}^{N_m}\left(\mathbf{f}_{\sigma,i}^{(n)} + \mathbf{f}_{\sigma,i}^{(t)}\right)$, $\mathbf{f}_{\sigma,i}^{(t)} = \delta_{\Gamma,i}^s\,\nabla_{\Gamma_i}\sigma$ is the Marangoni stress, σ is the surface-tension coefficient, $\nabla_{\Gamma_i}(\cdot)$ is the surface gradient, and $\delta_{\Gamma,i}^s = ||\nabla\phi_i||$ is a smoothed Dirac delta. Here, σ is constant; hence $\mathbf{f}_{\sigma,i}^{(t)} = \mathbf{0}$. The normal component is $\mathbf{f}_{\sigma,i}^{(n)} = \sigma\,\kappa_i\,\nabla\phi_i$ [4,5,6,7,9,8].

External mass transfer is modeled for the dissolved species concentration C in Ω_c:

$$\frac{\partial C}{\partial t} + \nabla\cdot(\mathbf{v}C) = \nabla\cdot(\mathscr{D}\nabla C)\,, \tag{3}$$

where $\mathscr{D} = \mathscr{D}_c$ is the diffusivity. The concentration inside the bubbles is constant. In cells intersected by the interface, C is interpolated as proposed in [7].

3 Numerical Experiments

Verifications, validations and extensions of the finite-volume UCLS method have been reported in our previuos research, for instance: rising bubbles [4,5], bubble swarms [3,7,9], droplet collision and droplet-interface interaction [3], droplet deformation [2,8], mass transfer in bubbly flows [7,9], variable surface tension [6,8], and liquid-vapor

ICCS Camera Ready Version 2026
To cite this paper please use the final published version:
DOI: 10.1007/978-3-032-29918-5_16

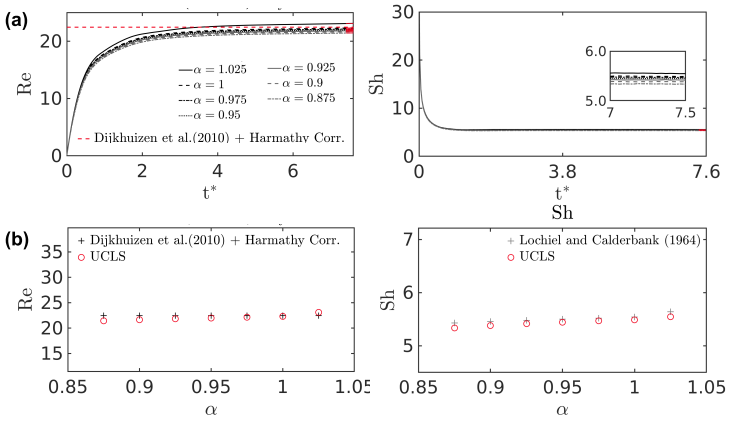

Fig. 2. Effect of interface thickness parameter $\varepsilon_P = 0.5\,\mathrm{h_P}^{\alpha}$ on gravity-driven rising bubble. $\mathrm{Eo} = 3.5$, $\mathrm{Mo} = 10^{-4}$, $\eta_\rho = \eta_\mu = 100$, $\mathrm{Sc} = 1$. (a) $\mathrm{Re}(\mathrm{t}^*)$) and $\mathrm{Sh}(\mathrm{t}^*)$. Terminal Re and Sh in red line. (b) Re and Sh from UCLS and correlations from [11] and [14], versus α. The Harmathy correction [13] is used for confinement effect on Re, using $d_b/D_\Omega = 0.125$.

phase change [1]. This work focuses on the role of the numerical interface thickness in the hydrodynamics and mass transfer in bubbles.

Transport equations are discretized by the unstructured collocated finite-volume method [7,9]. The unstructured TVD Superbee flux-limiter scheme solves the convective term as proposed in [7,9,4,8]. Central difference scheme for the diffusive term. Fractional-step projection method for the pressure-velocity coupling. The reader is referred to our previous research [7,9,8] for further technical details.

3.1 Computational setup and dimensionless parameters

Ω is a cylinder of diameter $D = 8d_b$ and axial length $L_y = 8d_b$. The mesh consists of 1.5372×10^6 hexahedral control volumes, with simulations executed on 112 CPU-cores. The mesh is refined around the cylinder axis ($h_{\min} \approx d_b/35$), consistently with our previous grid-convergence studies [2,5,7,9,8]. At the wall, a no-slip boundary condition is applied to $\mathbf{v}$, Neumann boundary conditions for ϕ_i and C. Periodic boundary conditions are enforced in the axial (y) direction. Initially, $\mathbf{v} = \mathbf{0}$.

Gravity-driven bubbles are characterized by the Morton number $\mathrm{Mo} = g\mu_c^4(\rho_c - \rho_d)\rho_c^{-2}\sigma^{-3}$, Eötvös number $\mathrm{Eo} = gd_b^2(\rho_c - \rho_d)\sigma^{-1}$, density and viscosity ratios $\eta_\rho = \rho_c/\rho_d$ and $\eta_\mu = \mu_c/\mu_d$, and Reynolds number $\mathrm{Re}_i(t^*) = \rho_c U_{r,i} d_b/\mu_c$, where $U_{r,i}$ is the bubble velocity relative to the carrier flow. Furthermore, $\mathrm{Re}(t^*) = N_b^{-1}\sum_{i=1}^{N_b}\mathrm{Re}_i(t^*)$, $\mathrm{Re}_i = T^{-1}\int_{t_0}^{t_0+T}\mathrm{Re}_i(t)\,dt$ and $\mathrm{Re} = N_b^{-1}\sum_{i=1}^{N_b}\mathrm{Re}_i$. In this research $N_b = 1$ and the dimensionless time is $t^* = t\,g^{1/2}\,d_b^{-1/2}$, where d_b is the spherical equivalent diameter. Mass transfer is characterized by the Schmidt number $\mathrm{Sc} = \mu_c/(\rho_c\mathscr{D}_c)$ and Sherwood number $\mathrm{Sh} = k_c d_b/\mathscr{D}_c$, k_c is the mass-transfer coefficient in Ω_c [7,9].

ICCS Camera Ready Version 2026
To cite this paper please use the final published version:
DOI: 10.1007/978-3-032-29918-5_16

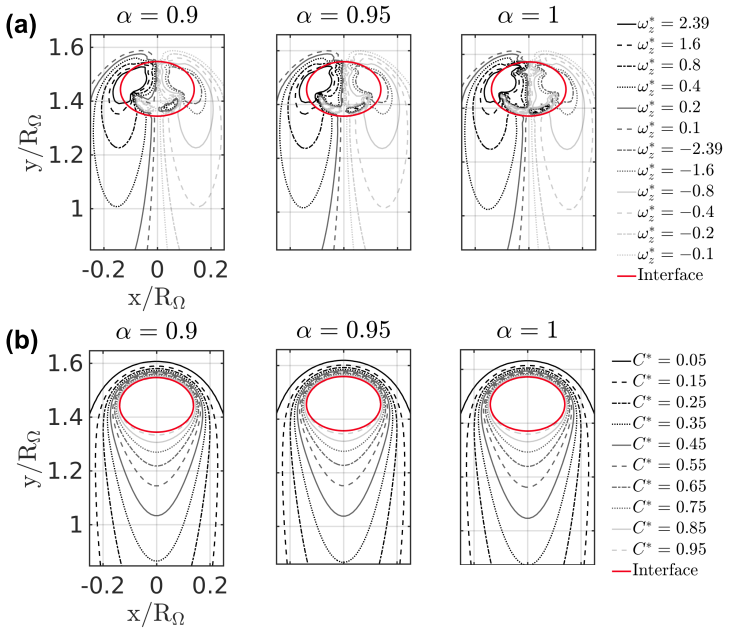

Fig. 3. Effect of interface thickness parameter $\varepsilon_P = 0.5\,\mathrm{h_P}^{\alpha}$ on gravity-driven rising bubble. $\mathrm{Eo} = 3.5$, $\mathrm{Mo} = 10^{-4}$, $\eta_\rho = \eta_\mu = 100$, $\mathrm{Sc} = 1$. (a) Vorticity ($\omega_z = \mathbf{e}_z \cdot (\nabla \times \mathbf{v})\,\sqrt{d_b/g}$)). (b) Concentration at $\mathrm{t}^* = 6.3$.

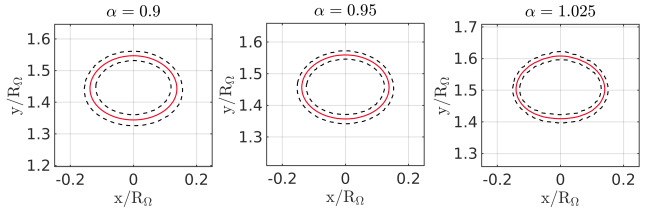

Fig. 4. Effect of interface thickness parameter $\varepsilon_P = 0.5\,\mathrm{h_P}^{\alpha}$ on gravity-driven rising bubble. $\mathrm{Eo} = 3.5$, $\mathrm{Mo} = 10^{-4}$, $\eta_\rho = \eta_\mu = 100$, $\mathrm{Sc} = 1$. UCLS marker profiles on the plane $x - y$ at $\mathrm{t}^* = 6.3$, $\phi = 0.5$ (red line) and $\phi = \{0.05, 0.95\}$ (discontinuous black line).

3.2 Interface-thickness sensitivity: single rising bubble

Figures 2–5 assess the sensitivity of UCLS-based DNS to $\varepsilon_P = 0.5\,h_P^{\alpha}$ at $\mathrm{Eo} = 3.5$, $\mathrm{Mo} = 10^{-4}$, $\eta_\rho = \eta_\mu = 100$, and $\mathrm{Sc} = 1$. Figure 2(a) reports $\mathrm{Re}(t^*)$ and $\mathrm{Sh}(t^*)$ for $0.875 \leq \alpha \leq 1.025$, with terminal values indicated by red lines. For all α, $\mathrm{Re}(\mathrm{t}^*)$ evolves from an initial acceleration stage to a well-defined terminal regime, while $\mathrm{Sh}(\mathrm{t}^*)$ exhibits an initial transient associated with the formation of the concentration boundary layer and then relaxes to a steady value. For reference, Re is compared with the correlation of [11] and the Harmathy correction [13].

ICCS Camera Ready Version 2026
To cite this paper please use the final published version:
DOI: 10.1007/978-3-032-29918-5_16

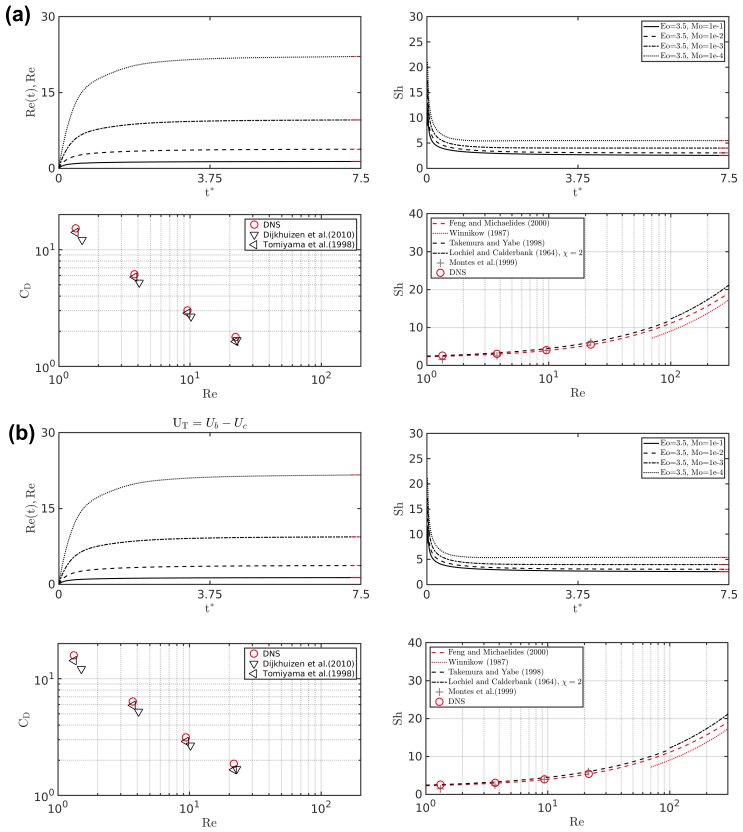

Fig. 5. Effect of interface thickness parameter (ε) on gravity-driven rising bubble. $\mathrm{Re}(\mathrm{t}^*)$, $\mathrm{Sh}(\mathrm{t}^*)$, $\mathrm{C_D}$ versus Re, Sh versus Re. $\mathrm{Eo} = 3.5$, $\mathrm{Mo} = \{10^{-1}, 10^{-2}, 10^{-3}, 10^{-4}\}$, $\eta_\rho = \eta_\mu = 100$, $\mathrm{Sc} = 1$. (a) $\varepsilon = 0.5\,{\mathrm{h_P}}^{0.975}$. (b) $\varepsilon = 0.5\,{\mathrm{h_P}}^{0.9}$.

Figure 2(b) summarizes the terminal Re and Sh as functions of α, comparing UCLS predictions with the references [11] (hydrodynamics) and [14] (mass transfer). For hydrodynamics, confinement is accounted for through the Harmathy correction [13] using $d_b/D_\Omega = 0.125$. Both Re and Sh exhibit a weak dependence on α. As α increases from 0.875 to 1, Re approaches the correlation of [11]; a similar trend is observed for Sh, which approaches the correlation of [14]. Overall, these results indicate that the diffuse-interface regularization primarily affects near-interface smoothing without introducing a significant bias in integral drag- and transfer-related predictions.

Fig. 3 compares vorticity and concentration fields at $t^* = 6.3$. The vorticity snapshots (Fig. 3(a)) show that the overall wake topology and shear-layer distribution are preserved when varying α, while the concentration fields (Fig. 3(b)) indicate that near-interface gradients and wake-mediated transport structures remain qualitatively consistent. Differences across α are mainly localized in the vicinity of the interface, consistent with the role of ε_P in regularizing material-property jumps and interfacial localization.

ICCS Camera Ready Version 2026
To cite this paper please use the final published version:
DOI: 10.1007/978-3-032-29918-5_16

Figure 4 provides a direct geometric measure of the numerical interface thickness through marker profiles on the x-y plane at $t^* = 6.3$. The interface is represented by $\phi = 0.5$ (red), whereas the iso-levels $\phi = \{0.05, 0.95\}$ (discontinuous black) provide a measure of the diffuse-layer width. This thickness regularization affects curvature evaluation, surface-tension forcing, and the smoothing of material properties across the interface. If $\alpha = 1.025$, small interfacial oscillations may be observed, indicating reduced numerical robustness in this configuration.

Figure 5 varies $\mathrm{Mo} = \{10^{-1}, 10^{-2}, 10^{-3}, 10^{-4}\}$, and compares two regularizations: $\varepsilon = 0.5\,h_P^{0.975}$ (Fig. 5(a)) and $\varepsilon = 0.5\,h_P^{0.9}$ (Fig. 5(b)). $\mathrm{Re}(t^*)$ and $\mathrm{Sh}(t^*)$, together with the parametric trends $\mathrm{C_D}(\mathrm{Re})$ and $\mathrm{Sh}(\mathrm{Re})$, are consistent with the reference correlations [11,12,17,16,14,15]. Overall, these results support that moderate variations in interface-thickness regularization preserve the integral hydrodynamic and mass-transfer scaling, while providing a practical handle to balance numerical robustness (curvature/capillary stability) and predictive accuracy.

4 Conclusions

This work assessed the sensitivity of UCLS-based DNS to the interface-thickness parameter $\varepsilon_P = 0.5\,h_P^{\alpha}$ in rising-bubble simulations with mass transfer. For $\mathrm{Eo} = 3.5$, $\mathrm{Mo} = 10^{-4}$, $\eta_\rho = \eta_\mu = 100$, $\mathrm{Sc} = 1$, $\mathrm{Re}(t^*)$ and $\mathrm{Sh}(t^*)$ reached well-defined terminal regimes for all α. Terminal Re and Sh showed a weak dependence on α and agreed with the correlations of [11,13] and [12,17,16,14,15], while wake topology and scalar-transport patterns remained similar, with differences near the interface. A Mo sweep confirmed that the expected trends in $C_D(\mathrm{Re})$ and $\mathrm{Sh}(\mathrm{Re})$ are preserved for $0.875 \leq \alpha \leq 1$, providing a balance between numerical robustness and predictive accuracy for $\mathrm{C_D}$ and Sh. The case with $\alpha = 1.025$ exhibits interface oscillations. Future work will extend this analysis to multiple bubbles, surfactants/Marangoni effects and liquid-vapor phase change.

References

1. Balcazar, N., Rigola, J., Oliva, A.: Unstructured level-set method for saturated liquid-vapor phase change. In: WCCM-ECCOMAS 2020. Volume 600 - Fluid Dynamics and Transport Phenomena. pp. 1–12 (2021). https://doi.org/10.23967/wccm-eccomas.2020.352, https://www.scipedia.com/public/Balcazar_et_al_2021a
2. Balcazar, N., Lehmkuhl, O., Jofre, L., Rigola, J., Oliva, A.: A coupled volume-of-fluid/level-set method for simulation of two-phase flows on unstructured meshes. Computers and Fluids **124**, 12–29 (2016). https://doi.org/10.1016/j.compfluid.2015.10.005, https://linkinghub.elsevier.com/retrieve/pii/S0045793015003394
3. Balcazar, N., Lehmkuhl, O., Rigola, J., Oliva, A.: A multiple marker level-set method for simulation of deformable fluid particles. International Journal of Multiphase Flow **74**, 125–142 (2015). https://doi.org/10.1016/j.ijmultiphaseflow.2015.04.009
4. Balcázar, N., Jofre, L., Lehmkuhl, O., Castro, J., Rigola, J.: A finite-volume/level-set method for simulating two-phase flows on unstructured grids. International Journal of Multiphase

ICCS Camera Ready Version 2026
To cite this paper please use the final published version:
DOI: 10.1007/978-3-032-29918-5_16

Flow **64**, 55–72 (2014). https://doi.org/10.1016/j.ijmultiphaseflow.2014.04.008
5. Balcázar, N., Lehmkuhl, O., Jofre, L., Oliva, A.: Level-set simulations of buoyancy-driven motion of single and multiple bubbles. International Journal of Heat and Fluid Flow **56**, 91–107 (12 2015). https://doi.org/10.1016/j.ijheatfluidflow.2015.07.004
6. Balcázar, N., Rigola, J., Castro, J., Oliva, A.: A level-set model for thermocapillary motion of deformable fluid particles. International Journal of Heat and Fluid Flow **62**, 324–343 (12 2016). https://doi.org/10.1016/j.ijheatfluidflow.2016.09.015, https://linkinghub.elsevier.com/retrieve/pii/S0142727X16301266
7. Balcázar-Arciniega, N., Antepara, O., Rigola, J., Oliva, A.: A level-set model for mass transfer in bubbly flows. International Journal of Heat and Mass Transfer **138**, 335–356 (8 2019). https://doi.org/10.1016/j.ijheatmasstransfer.2019.04.008
8. Balcázar-Arciniega, N., Rigola, J., Oliva, A.: Unstructured conservative level-set method for two-phase flows with insoluble surfactants. International Journal of Heat and Mass Transfer **261** (6 2026). https://doi.org/10.1016/j.ijheatmasstransfer.2026.128547
9. Balcázar-Arciniega, N., Rigola, J., Pérez-Segarra, C.D., Oliva, A.: Numerical study of the drag force, interfacial area and mass transfer in bubbles in a vertical pipe. Chemical Engineering Journal **495**, 153124 (9 2024). https://doi.org/10.1016/j.cej.2024.153124, https://linkinghub.elsevier.com/retrieve/pii/S1385894724046126
10. Brackbill, J.U., Kothe, D.B., Zemach, C.: A continuum method for modeling surface tension. Journal of Computational Physics **100**, 335–354 (1992). https://doi.org/10.1016/0021-9991(92)90240-Y, https://linkinghub.elsevier.com/retrieve/pii/002199919290240Y
11. Dijkhuizen, W., Roghair, I., Annaland, M.V.S., Kuipers, J.: Dns of gas bubbles behaviour using an improved 3d front tracking model—drag force on isolated bubbles and comparison with experiments. Chemical Engineering Science **65**, 1415–1426 (2 2010). https://doi.org/10.1016/j.ces.2009.10.021
12. Feng, Z., Michaelides, E.E.: Mass and heat transfer from fluid spheres at low reynolds numbers. Powder Technology **112**, 63–69 (10 2000). https://doi.org/10.1016/S0032-5910(99)00306-X, https://linkinghub.elsevier.com/retrieve/pii/S003259109900306X
13. Harmathy, T.Z.: Velocity of large drops and bubbles in media of infinite or restricted extent. AIChE Journal **6**, 281–288 (6 1960). https://doi.org/10.1002/aic.690060222, https://aiche.onlinelibrary.wiley.com/doi/10.1002/aic.690060222
14. Lochiel, A., Calderbank, P.: Mass transfer in the continuous phase around axisymmetric bodies of revolution. Chemical Engineering Science **19**, 471–484 (7 1964). https://doi.org/10.1016/0009-2509(64)85074-0
15. Montes, F., Galan, M., Cerro, R.: Mass transfer from oscillating bubbles in bioreactors. Chemical Engineering Science **54**, 3127–3136 (7 1999). https://doi.org/10.1016/S0009-2509(98)00314-5, https://linkinghub.elsevier.com/retrieve/pii/S0009250998003145
16. Takemura, F., Yabe, A.: Gas dissolution process of spherical rising gas bubbles. Chemical Engineering Science **53**, 2691–2699 (8 1998). https://doi.org/10.1016/S0009-2509(98)00094-3
17. Winnikow, S.: Letter to the editors. Chemical Engineering Science **22**, 477 (3 1967). https://doi.org/10.1016/0009-2509(67)80138-6

ICCS Camera Ready Version 2026
To cite this paper please use the final published version:
DOI: 10.1007/978-3-032-29918-5_16